Proceedings of ASME Turbo Expo 2011
GT2011
June 6-10, 2011, Vancouver, British Columbia, Canada

GT2011-46470

GAS TURBINE EMISSION CHARACTERISTICS IN PERFECTLY PREMIXED COMBUSTION

A. M. Elkady, D. M. Kalitan, J. Herbon, and G. Leonard
Energy and Propulsion Technologies
GE Global Research Center
Niskayuna, NY, USA

R. Akula
BEC-ATO, GE Energy
JFW Technology Center
Bangalore, India

H. Karim, M. Hadley
GE Energy
Greenville, SC, USA

ABSTRACT

In the present study, a simple perfectly premixed research burner was utilized at temperatures, pressures and residence times representative of an industrial gas turbine cycle to identify the lower limit of NO_x and CO emissions, and to establish an emissions benchmark for practical gas turbine combustors. In addition to experimental data, a chemical reactor model has been utilized for the prediction of the NO_x and CO, based on detailed chemical reaction mechanisms. Several current kinetics mechanisms were evaluated and subsequently compared to the experimental data. In addition, sensitivity analysis was performed to identify important reactions at the conditions tested, and will be discussed.

INTRODUCTION

As the acceptable limit of emissions production in industrial gas turbine decreases, it is important to identify the lower limit at which traditional gas turbine combustors can be operated and achieve acceptable levels of NO_x and CO. The typical trend in NO_x reduction techniques has been to decrease the combustor primary zone flame temperature, reduce the residence time of the combustor and move towards more perfectly premixed fuel and air conditions. These are all used effectively; however, when these approaches are examined in industrial gas turbine nozzles it is often difficult to isolate out one effect from the other. Therefore, it is difficult to determine what the most prominent driving effect on NO_x and/or CO emissions truly is. Using a simple perfectly premixed combustor at temperatures and pressures representative of an industrial gas turbine will enable the evaluation of current kinetic mechanism for model validation.

Well-controlled, perfectly premixed combustion experiments are often utilized to evaluate emissions and flammability limits [1-5]. Perfectly premixed combustion experiments avoid the additional complexity and uncertainty in mixedness that is typically present in industrial gas turbine combustion systems. This allows the isolated study of the flame chemistry and provides the opportunity to test detailed chemical kinetic mechanisms. Furthermore, simple burner geometries, which produce limited mixing or recirculation zones, allow fairly simplified models to be coupled with the detailed chemical mechanisms and used to evaluate and compare model predictions with experimental results. Several authors have reported the results of perfectly premixed flames at typical gas turbine pressures and temperatures. Studies by Cheng and coworkers [3-5] have successfully used a low-swirl injector (LSI) concept to produce very low emissions flames in both natural gas and syngas fuels. However in this study, the swirl component was eliminated to isolate its effect on NO_x production due to the presence of the recirculation zone.

This study examines the combustion of perfectly premixed typical pipeline natural gas in air at conditions representative of industrial gas turbines, both experimentally and numerically. The goal of the experiments was to generate an emissions database for perfectly premixed combustion, and a) determine the lowest NO_x emissions that could be achieved, b) determine the dependency of emission formation on different operating parameters, such as inlet pressure, inlet temperature

and residence time, and c) compare against current chemical kinetics models.

This study is a continuation of the work initially performed by Leonard and Correa [1], by extending the test conditions and range of fuels. Leonard and Correa examined NO_x formation for perfectly premixed methane/air flames from 1-10 atm and compared their experimental results to the Glarborg et al. [6] chemical kinetics mechanism using reactor network modeling. The work herein was conducted for natural gas/air flames for pressures up to approximately 16 atm. Detailed chemical kinetic modeling was completed and compared to the experimental results over a representative range of conditions.

EXPERIMENTAL SETUP

The goal of the current study was to examine the effects of different operating parameters such as pressure, inlet temperature, and residence time on emissions production. A pressure vessel with a diameter of 20.32 cm and rated to operate up to pressures of 20.4 atm at 728K was utilized as shown in Figure 1. The pressure vessel had optical access capability to visualize the flame. In order to ensure that the fuel and air were well premixed upstream of the combustor inlet, fuel and air were premixed in a 1.27cm diameter tube with a length greater than 200 tube diameters. The fuel utilized was a typical pipeline natural gas and was available through on-site facilities and was composed of the constituents listed in Table 1 at the time of the experiments.

Preheated air at pressures ranging from 6.8-16.3 atm was utilized to provide both combustion and liner cooling air. The total preheat air mass flow rate ranged between 0.27-0.55 kg/sec depending on the operating conditions. As shown in Figure 1, the preheated combustion air was mixed with ambient temperature natural gas upstream of the pressure vessel and prior to entering the mixing tube bundle. The preheated air used for combustor cooling was also utilized to preheat the fuel/air mixture outside the tube bundle. The fuel/air mixture temperature and pressure were measured just upstream of the flame arrestor as presented in Figure 1.

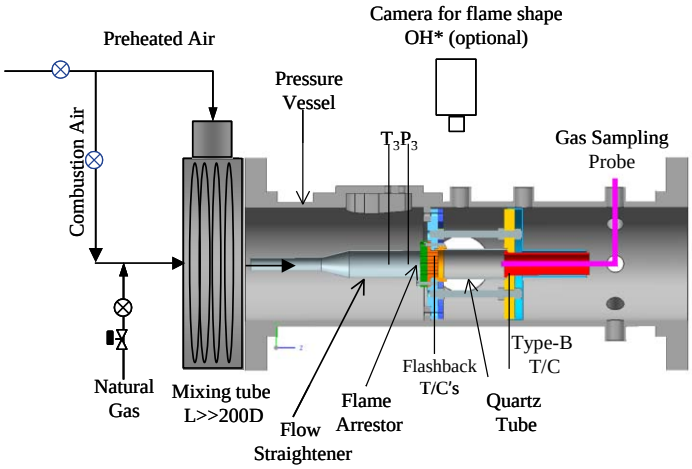

Figure 1. Experimental setup

Table 1: Experimental natural gas composition

Composition	Mole Fraction (%)
Methane	96.331
Ethane	1.543
Propane	0.215
Nitrogen	1.016
Carbon Dioxide	0.771
I-Butane	0.031
N-Butane	0.036
I-Pentane	0.027
N-Pentane	0.009
C6+	0.021

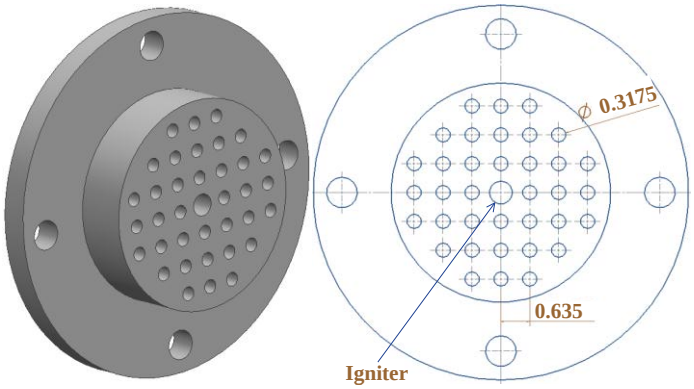

Figure 2. Perforated plate design. Dimensions are in [cm]

The combustor used in this study consists of a quartz liner with a length of 10.67 cm and diameter of 5.08 cm. A quartz liner was utilized for the benefit of having optical access to characterize the flame, check the flame shape at different conditions and to interpret the changes in combustion acoustics and flame shape. The flame was stabilized downstream of a perforated plate which was designed similar

to the one studied by Leonard and Correa [1]. The perforated plate was made of 1.91 cm thick Hast-Alloy X and had 36 holes arranged as shown in Figure 2. Each hole had a diameter of 0.3175 cm. Ignition was established using a high voltage spark unit. The igniter was positioned in the center of the perforated plate. Upstream of the perforated plate was a stainless steel flame arrestor that had 36 holes, 0.15875 cm in diameter. The plate was also instrumented with thermocouples to detect flashback and flame holding events.

Experiments were conducted over a range of conditions to investigate the effect of various operating parameters. Pressure ranged from 6.8 to 16.32 atm, combustor adiabatic flame temperatures were examined from near lean blow-out (LBO) up to 2144 K. Combustor residence time was also varied from 10 to 20 milliseconds.

Combustion air was metered using a venturi with accuracy less than 1.5%. Fuel was metered using a coriolis type mass flow meter with accuracy of about 0.5%. Combustion products were sampled using a water-cooled gas sampling probe, placed 10.6 cm downstream of the perforated plate face. The sample was then transferred to the sample-conditioning unit via a heated line passing through a heated filter. A stream of the sample was then cooled, dried, and analyzed in a California Analytical gas sampling system for CO_2, O_2, UHC, and CO measurement. The other stream remained heated before entering the NO_x analyzer to eliminate loss of NO_2 that is soluble in water if the sample was cooled and the water was able to condense.

The gas sampling unit was calibrated using standard calibration gases. The analyzers were spanned before the test then checked during and after the experiments to confirm precision of the measurements. A gage repeatability and reproducibility analysis has been performed on the NO_x analyzer and confirmed measurement accuracy of the device is within 1ppm (without correction) of the full range. NO_x emissions are corrected and reported to a 15% O_2 level by volume.

It is important to note that the flame temperatures reported in this study are calculated values and can be determined by several different methods. Either it can be calculated based on the metered flow measurement of fuel and air into the combustor ($T_{flame,\ flow}$), or it can be calculated based on the sampled emissions at the exit of the combustor. The measured species typically used for this calculation are O_2, or CO_2 when complete combustion assumptions are valid. Flame temperature based on O_2 and CO_2 typically match to within 0.5% when the assumption of complete combustion is satisfied. In this work, the experimental temperatures reported are calculated based on O_2 concentrations.

Chemical Kinetic Modeling

Detailed chemical kinetic modeling was utilized to predict the NO_x and CO generated during combustion. The fuel/air mixture used in this study was perfectly premixed before entering the perforated plate combustor. Since this type of burner does not introduce significant turbulence to the flow, a simple reactor network could be utilized in Chemkin™ to model the combustion chemistry. Using the reactor network shown in Figure 3, the combustion characteristics of natural gas in air were simulated using several modern chemical kinetics mechanisms. The network consists of an inlet, a Perfectly Stirred Reactor (PSR) and a Plug Flow Reactor (PFR).

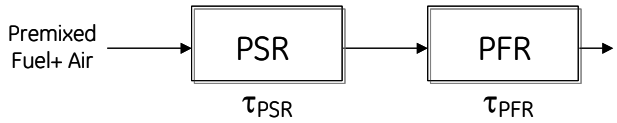

Figure 3. Chemical kinetic reactor network for flame simulation

To determine the emissions characteristics for natural gas at the relevant conditions, the inlet parameters listed in Table 2 were used as input to the reactor network. In addition to the temperature, pressure and mass flow rate of the system the residence times of the PSR and PFR were specified. The summation of the PSR and PFR residence times equate to the total system residence time.

$$\tau_{Total} = \tau_{PSR} + \tau_{PFR} \tag{1}$$

This overall residence time was matched to the actual experimental total residence time and was 22 ms on average for the baseline case. The PSR time is related to the reaction front in the flame zone and was chosen to be equal to the chemical time scale of the flame. This chemical time scale (τ_{CTS}), is defined as the ratio of the flame thickness to the laminar flame speed

$$\tau_{CTS} = \frac{\left(\lambda / C_p\right)_{T_O}}{\rho_u S_L^{\ 2}} \tag{2}$$

where T_O is the inner-layer temperature in (K), ρ_u is the unburned gas density (kg/m^3) and S_L is the laminar flame speed (m/s). The inner layer temperature was defined to be the average of the burned and unburned gas temperatures. Subsequently, a parameter study was conducted in the reactor network by varying the equivalence ratio, the PSR time and the PFR time in order to cover the entire operating space.

Table 2: Run conditions for NO_x and CO emissions chemical kinetics calculations

Inlet Parameter	Unit	
Phi		0.4 - 0.75
Comb Air Mdot	[kg/s]	0.023
T3	[K]	633.2
P3	[atm]	12.39
Combustor Length	[cm]	11.38
Combustor Diameter	[cm]	5

NO_x Chemical Kinetics

Several current chemical kinetics mechanisms shown in Table 3 were utilized in the reactor network and compared to the experimental data. It is important to note here that three of the six mechanisms studied did not contain a NO_x sub-mechanism. For the purposes of this study the NO_x sub-mechanism of the GRI-Mech 3.0 [7] was added to the Dooley et al. [8], Healy et al. [9] and Wang et al. [12] mechanisms. They will herein be referred to as modified versions of the original mechanisms.

Table 3: List of chemical kinetics mechanisms

Mechanism	NOx Chemistry
GRI-Mech 3.0 [7]	Yes
Dooley et al. [8]	No
Healy et al. [9]	No
Kintech Mech [10]	Yes
Ranzi et al. [11]	Yes
Wang et al. [12]	No

RESULTS AND DISCUSSIONS

As mentioned previously, the current study is an extension of the work completed by Leonard and Correa [1], hereafter solely referred to as Leonard and Correa. To ensure that the experimental facility was consistent between the current study and the work performed previously [1], several test cases from Leonard and Correa were replicated to ensure that similar NO_x values could be obtained before moving on to the current fuels and conditions of interest. For these replicated test points, perfectly premixed conditions were achieved using bottled methane as the fuel. Figure 4 shows the results from this repeatability study. Agreement between the two studies was achieved which increased the level of confidence in the current experimental configuration.

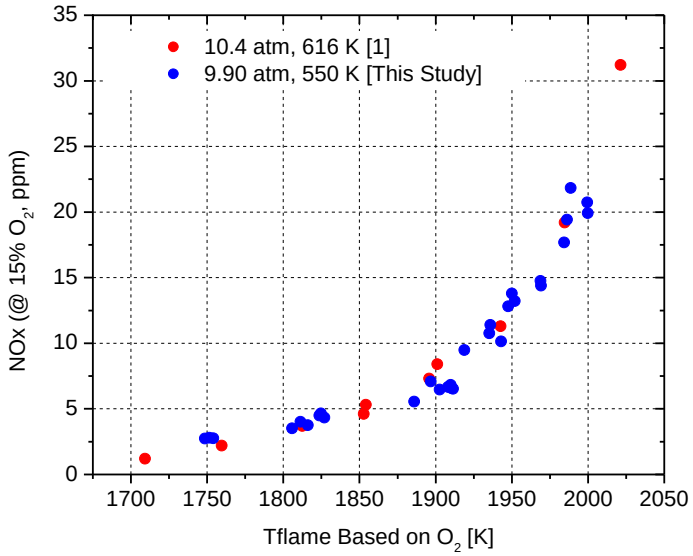

Figure 4. NO_x emissions as function of flame temperature. Comparison with Leonard and Correa. [1]

Figure 5 shows results which are representative of an E-Class gas turbine operating at P_3~12.58 atm, and T_3~ 633K with a residence time corresponding to ~20 msec at combustor exit. At these conditions, it is clear that single digit NO_x could be achievable at flame temperatures less than 1900K. Generally, most of the NO_x created at flame temperatures less than 1900K is attributed to prompt NOx while thermal NO_x becomes more significant at temperatures greater than 1866K.

Results of the NO_x chemical kinetic analysis using the GRI-Mech 3.0 [7] are also shown in Figure 5 and can be compared to the experimental data. It is worth noting that the flame temperature reported on the x-axis is the adiabatic flame temperature for the modeled data and is the temperature based on O_2 emissions measurements for the experimental data. It is clear from the comparison that the mechanism and the data do not agree well over the entire temperature range. At times the model over-predicts the experimental data by almost a factor of two. Although the model does not capture the NO_x values accurately, the overall trend in NO_x production is modeled well by the mechanism as it transitions from prompt NO_x to the thermal NO_x pathways.

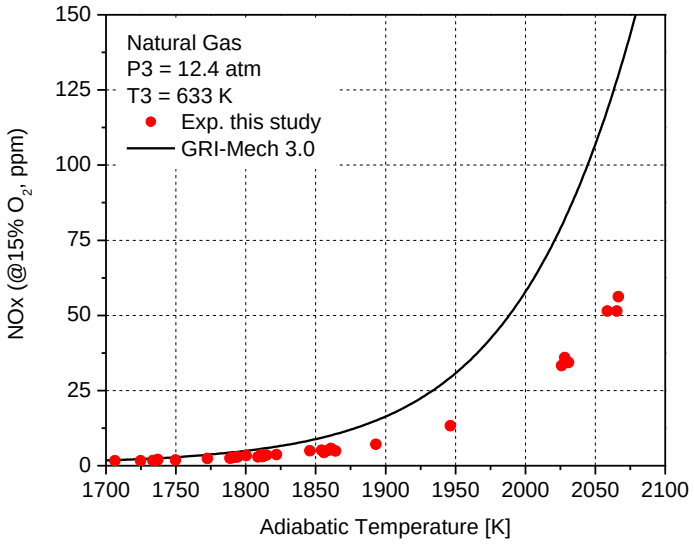

Figure 5. NO_x emissions at P_3~12.58 atm, T_3~688K, and τ~20 msec compared to GRI-Mech 3.0 [7] model

Heat-Loss Analysis

There are several possible explanations for the disagreement between the chemical kinetic model results and the experimental data shown in Figure 5: 1) The PSR+PFR reactor network model shown in Figure 4 is not an accurate physical model of what is occurring in the combustor 2) The actual reactor network model was a valid assumption but the choice of residence time splits between the PSR and PFR were erroneous or the assumption of using the chemical timescale for the PSR time was not correct 3) Inaccuracies in the chemical kinetic rate of reactions 4) The assumption of adiabatic combustion could be inaccurate due to heat loss occurring along the length of the combustor (quartz liner) such that the temperature at the entrance to the emissions probe was not the adiabatic flame temperature.

A subsequent analysis of the results indicated that the most likely reason for the disagreement between the NO_x experimental results and the chemical kinetic mechanism results occurred due to the heat loss along the quartz combustor walls. The reason for selecting the quartz was purely for the benefit of having optical access to characterize the flame, check the flame shape at different conditions and to interpret the changes in combustion acoustics with flame shape. A simple 1-D model has been developed to quantify the heat loss along the length of the combustor and enabled the calculation of the combustor exit temperature at the probe sampling location. As depicted in Figure 6a, the heat loss model included radiation, inner and outer convection and conduction. The pressure vessel walls were considered to be far away from the liner in order to satisfy the assumption that the preheated air volume around the liner could be considered infinite. Emission was modeled as grey body emission. To simplify the model it was assumed that the flame reached the adiabatic flame temperature immediately after the PSR region. Following this peak, the temperature decreases due to heat losses and reached the combustor exit temperature at the probe sampling location. To ensure the accuracy of the heat loss model, the test section was instrumented with thermocouples as shown in Figure 6b.

As shown in Figure 7, applying heat loss corrections to the experiments, and comparing on the basis of the combustor exit temperature rather than using adiabatic flame temperature, better agreement can be achieved between the experimental data and the GRI-Mech 3.0 mechanism[7].

Chemical Kinetic Mechanisms Comparison

The GRI-Mech 3.0 [7] has been the industry standard for many years however; there has been several recent natural gas kinetic models published with updated reaction rates [8-12]. These updated rates have improved model agreement to fundamental data such as ignition delay time and laminar flame speed experiments. For the current study, the six mechanisms listed in Table 3 were utilized to compare chemical kinetic predictions of NOx production to experimental data and to compare the performance of each individual mechanism to the GRI-Mech 3.0 [7]. Figure 8 shows the results of the non-adiabatic model comparisons to the heat loss corrected data. The heat loss corrected data shown in Figure 8 are the same as those shown in Figure 7 however, the temperature range has been decreased in Figure 8 to draw more attention to the lower temperature regime where DLN combustors are typically operated. Overall, the models capture the trends of the data as the production of NOx increases with flame temperature. In particular, the Kintech mechanism [10] performs best in the mid to lower temperature compare the performance of each individual mechanism to the GRI-Mech 3.0 [7].

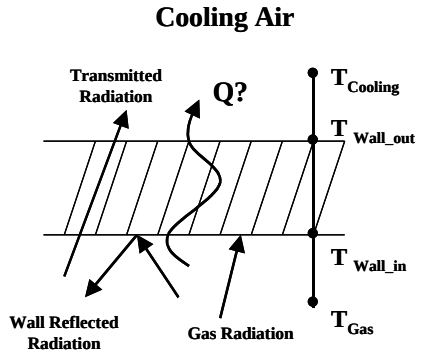

a. Heat Loss model used to represent the experiment

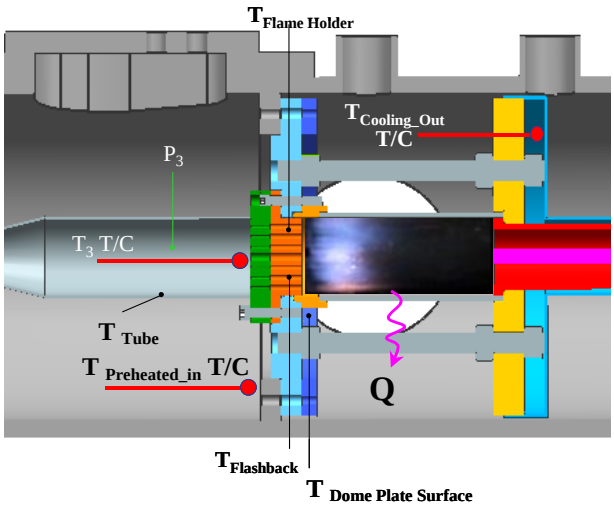

b. Test section instrumentation for quantification of heat losses

Figure 6. Combustor heat loss analysis

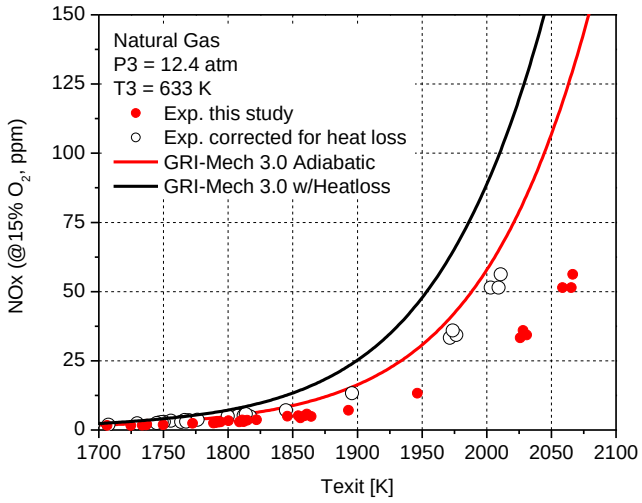

Figure 7. Comparison of the data and model [7] after accounting for the heat loss through the combustor walls

Figure 8 shows the results of the non-adiabatic model comparisons to the heat loss corrected data. The heat loss corrected data shown in Figure 8 are the same as those shown in Figure 7 however, the temperature range has been decreased in figure 8 to draw more attention to the lower temperature regime where DLN combustors are typically operated. Overall, the models capture the trends of the data as the production of NOx increases with flame temperature. In particular, the Kintech mechanism [10] performs best in the mid to lower temperature range (1700-1800K) while the GRI-Mech 3.0 [7] shows good agreement below 1800K as well.

As mentioned previously, the regulated emissions limits for NO_x generation in gas turbine combustors are continually being decreased. The desire to design and operate gas turbine combustors below 10 ppm also requires accurate chemical kinetic models to predict the combustion. It is quite interesting to observe that the concentration of NOx predicted over the entire temperature range presented in Figure 8 is quite large from model to model; making accurate prediction of NOx difficult, especially at lower flame temperatures. Comparing the

Performance of the mechanisms at the lowest flame temperature (1700K), there is a factor of two disagreement in the prediction of NOx between the Kintech Mech [10] and the Dooley et al. modified mechanism [8]. As the temperature increases, the agreement among the models improves but all of the mechanisms over-predict the NOx at higher flame temperatures. Beyond accounting for the heat lost through the combustor walls, the reason for the disagreement is not known at this point and is the subject of future studies.

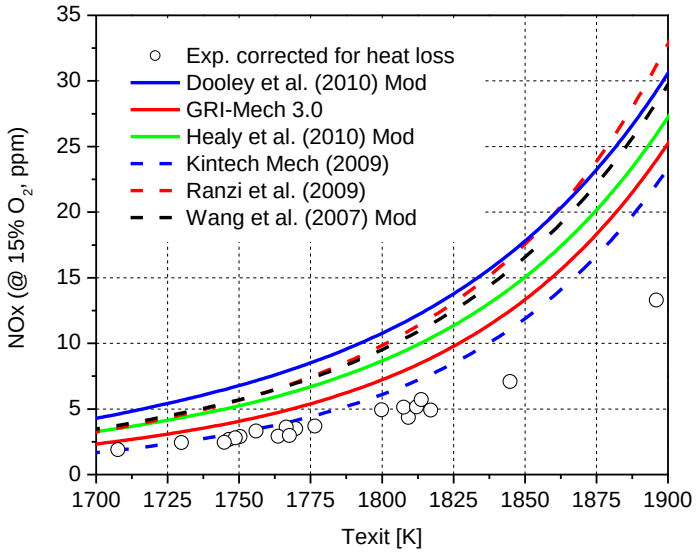

Figure 8. Comparison of heat loss corrected chemical kinetics mechanisms [7-12] and experimental data at conditions listed in Table 2

Pressure Effects

In order to quantify the effect of pressure on NOx production, NOx emission data was collected at two distinct pressures (8.16 atm and 16 atm) and the results are shown in Figure 9a. Although the initial temperature for the two cases was slightly different, a subsequent sensitivity study was completed and indicated that inlet temperatures within the examined range did not affect NO_x production. Examination of Figure 9a indicates that the effect of pressure on NO_x production may appear less significant at temperatures below 1866K. However, in cases where the flame temperatures are higher than 1866K, the effect of pressure on thermal NO_x production is quite significant. Using the relation that NO_x scales with pressure as P^n, it is clear that n increases with flame temperature and is not a constant factor as suggested in other publications (e.g. Lefebvre [13]). For example, at a flame

temperature of 1894K, the value of n is approximately 0.38 while at 1977K, the value of n is about 0.53. Results confirm that the pressure effect on NO_x is significant at higher firing temperatures and care must be taken when transferring or scaling results of experiments operated at low pressures to high pressures representative of gas turbine combustors.

In addition to the experimental results presented in Figure 9a, the effects of pressure on the production of NOx relative to flame temperature were modeled using the GRI-Mech 3.0 [7]. The modeling results shown in Figure 9b show similar trends to those presented in Figure 9a. The trends observed in these plots indicate that increasing pressure will cause the flame thickness to decrease. The decrease in flame thickness will result in a slight increase of NO_x in the flame zone due to rapid thermal NO_x production. Conversely, in the post flame region the production rate of NOx increases with pressure and can be understood by analyzing the reaction rates of production shown in Figure 10. The rate of production of NOx with respect to the thermal NOx mechanism is plotted for 8.16 atm and 16 atm. The figure indicates increasing rates of production for all three reactions at higher pressures.

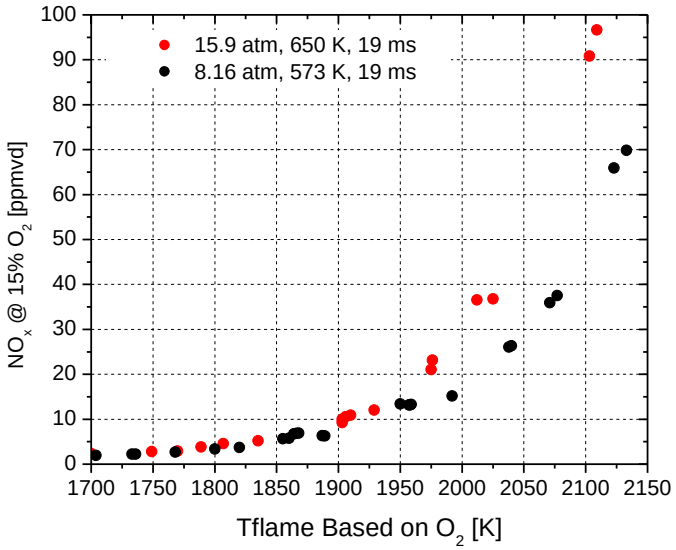

a. Experimental results.

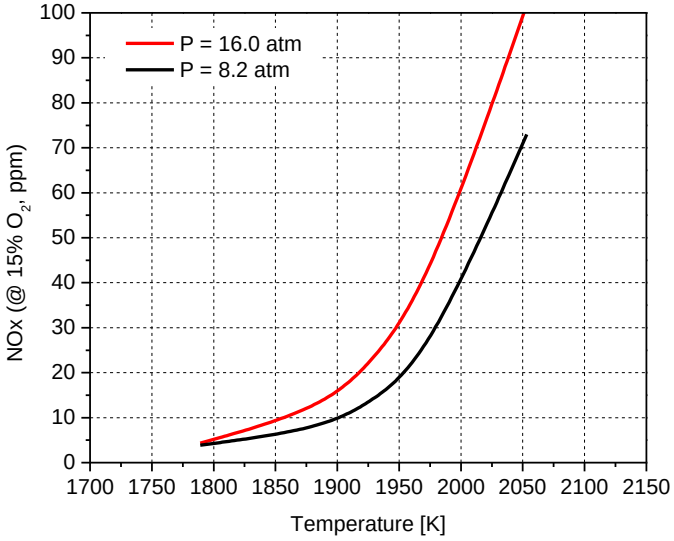

b. Model results

Figure 9. Effect of pressure on NOx production.

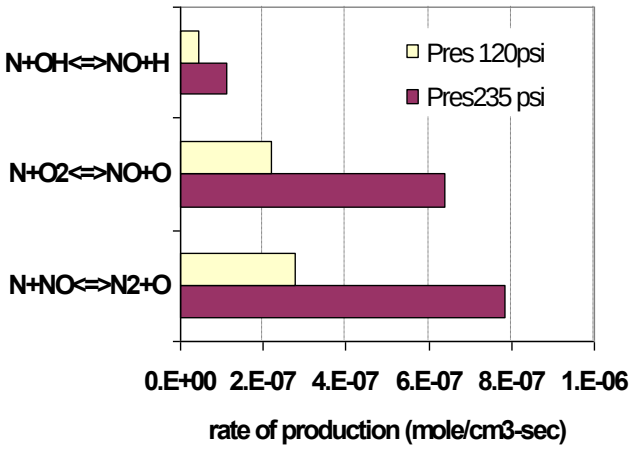

Figure 10. Pressure Effect on ROP of NOx

Residence Time Effect

In addition to pressure effects, the residence time effect on NOx production was studied over a range of flame temperatures. Experimental results are presented in Figure 11a while the GRI-Mech 3.0 [7] was used to produce the results in Figure 11b. In both cases, the inlet pressure was fixed at P3 = 8.16 atm, and the inlet temperature was T3 = 572K. The combustor residence time was varied between 10 and 20 msec. Varying the mass flow rate of the reactants changed the residence time of the hot gases in the combustor. Therefore, the effect seen here on NO_x may not solely be due to changes in residence time but also may be due to changes in reactant velocities.

From the figures it is clear that the experiments and the model are capturing the trends well. It is also clear that the

residence time effect becomes more prominent at temperatures higher than 1866K. For example at a temperature of 1977K, the rate of increase in NOx is about 0.7 ppm per millisecond. This rate of NOx production decreases significantly to 0.2 ppm per millisecond at a temperature of 1866K.

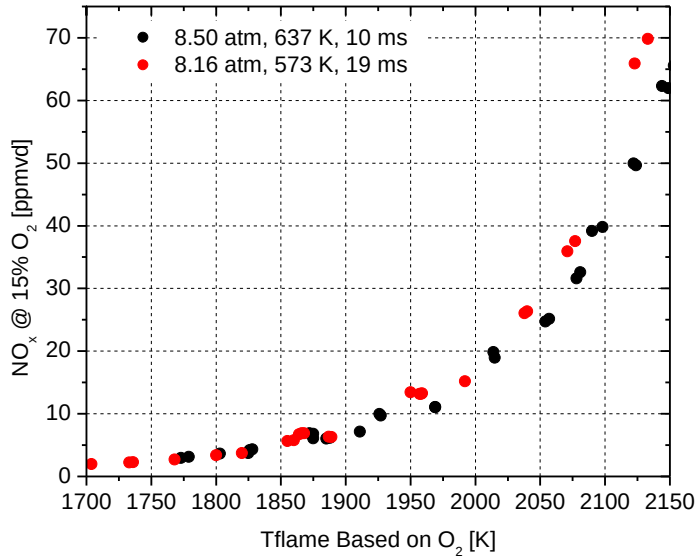

a. Experiments results

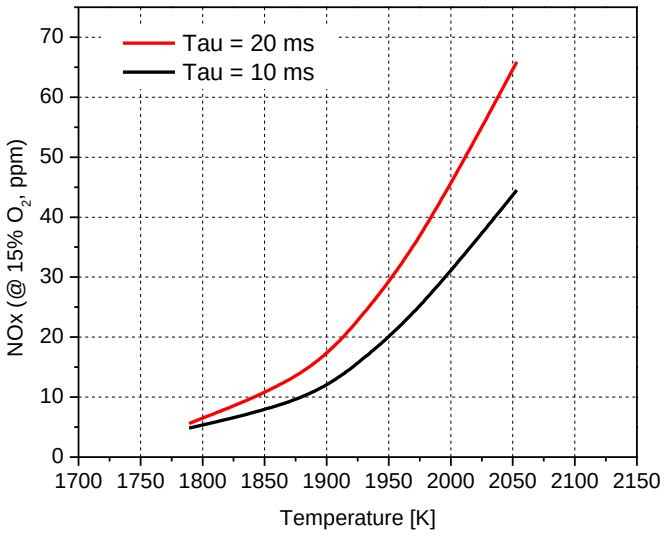

b. Model results

Figure 11. Effect of Residence time on NO_x production

CO Experimental Emissions

In this work, a simple water-cooled probe was utilized for sampling combustion exhaust gas at the exit of the quartz combustor. In order to measure accurate CO emissions, the exhaust gases must be quenched immediately upon entering the sample probe to avoid the continuation of the transition of CO to CO_2. Although a water-cooled probe was utilized in the current study, a thorough analysis of the actual quenching time was not completed and therefore, some minor reaction progress could have occurred for some short distance down the length of the probe. Therefore, the CO data presented herein should be used as a means for examining the trends in CO formation relative to flame temperature and should not be evaluated as an absolute value of CO produced inside the combustor.

Experimental data of CO emissions (corrected to 15% O_2) are presented as a function of calculated adiabatic flame temperature in Figure 12. High CO concentrations are found at very low flame temperatures (below 1755K) due to flame stability as the LBO limit is approached. As the flame temperature is increased and the flames stabilize, the CO decreases. CO values continue to decrease due to the oxidation reaction CO + OH → CO_2 + H which becomes significant at higher temperatures, reaching a minimum at about 1783-1810K. Beyond a flame temperature of 1800K the dissociation of CO_2 to CO occurs and leads to an increase in CO concentrations at the combustor exit. Figure 12 also shows the effect of pressure on CO production. It is clear that pressure is effective only in the region where CO is increasing with flame temperature due to dissociation. It is apparent here that increasing pressure shifts the equilibrium from CO to CO_2, as expected. However, in the low temperature regions, increasing combustion pressure does not lead to an acceleration of the conversion of CO to CO_2.

In addition to pressure effects on CO emissions, residence time effects were also studied and results are shown in Figure 13. As the residence time increases, more CO can complete the conversion to CO_2 in the low temperature region. However, once the temperature is high enough (beyond ~1866K) the effect of residence time becomes less significant.

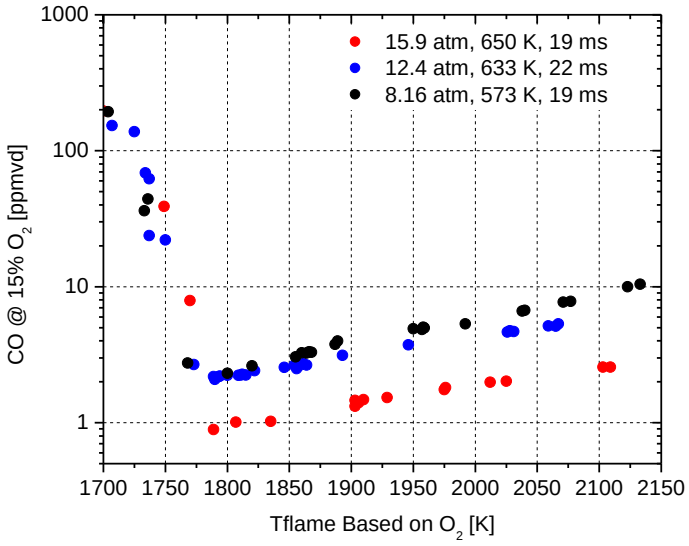

Figure 12. Effect of pressure on CO emission

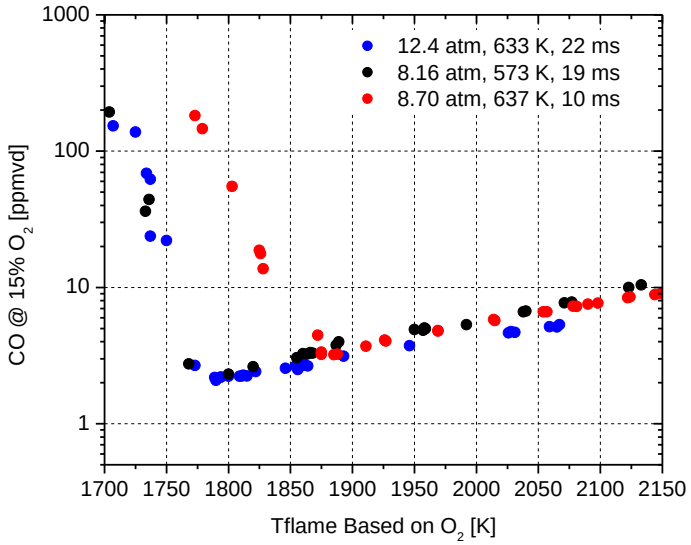

Figure 13. Effect of residence time on CO emissions.

CO Chemical Kinetics

Following the NOx chemical kinetic analysis, the CO experimental results were compared against the GRI-3.0 mechanism [7] and are shown in Figure 14. The two different CO experimental results shown in the figure represent the data with and without correction for heat loss through the quartz combustor walls. It is apparent from the figure that there is no agreement between the model and the data over the entire operating range. As mentioned previously, measured CO values may not represent the true concentrations in the combustor due to probe cooling effects. At high temperatures, the adiabatic model predicts that CO quickly reaches a steady state concentration, i.e. thermochemical equilibrium. Interestingly, in addition to the GRI-30 mechanism, the six chemical kinetic mechanisms [8-12] listed in Table 3 were also tested but yielded the exact same results (i.e., the equilibrium values of CO combustion) and therefore were not plotted in Figure 14 for simplicity.

CONCLUSIONS

This study provides engine-relevant NO_x and CO emissions produced by a simple perforated-plate burner geometry. A PSR-PFR reactor network was configured to model the combustion emissions of natural gas in air. Results of the NOx and CO numerical analyses were compared to the experimental results. The relative trends of NO_x production were modeled well and improved agreement between the experiment and models were achieved once heat loss through the combustor was considered. The chemical kinetic calculations of CO predict thermochemical equilibrium and did not agree with the experimental data; however, the CO measurements are likely impacted by sample probe cooling effects.

Pressure and residence time effects on NOx production were studied experimentally and numerically. Increasing pressure and residence time increased NOx generation, especially at higher flame temperatures. NOx emissions, while historically thought to be proportional to P^n with n = constant, were found to have a temperature-dependent value of n. The present study attempted to focus on certain combustor parameters (pressure and residence time) in the absence of effects such as unmixedness and strong recirculation zones, thus comparing more directly the sensitivity of chemical kinetic NOx production to those parameters.

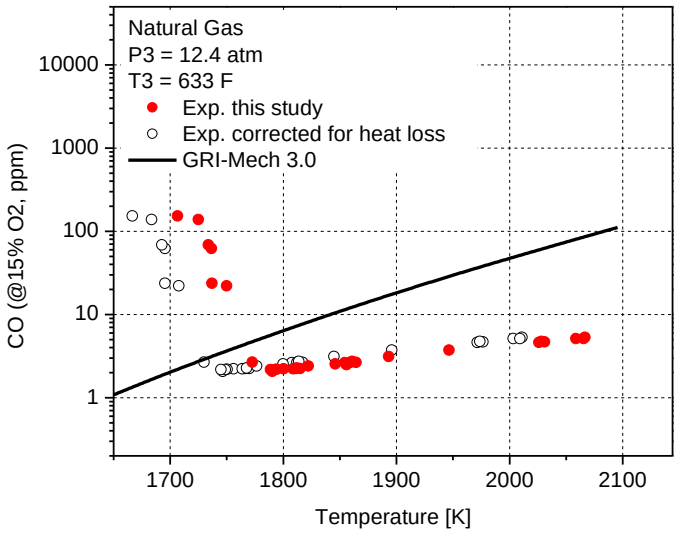

Figure 14. Comparison of CO experimental and modeled results

ACKNOWLEDGMENTS

Dr. Mohamed Sakami and Dr. Hejie Li are acknowledged for their insight and assistance to this study.

REFERENCES

(1) Leonard, G., and Correa, S., 1990, "NOx Formation in Premixed High-Pressure Lean Methane Flames," Fossil Fuel Combustion Symposium: 13th Annual Energy-Sources Technology Conference and Exhibition, New Orleans, pp. 69-74.

(2) Johnson, M. R., Littlejohn, D., Nazeer, W.A., Smith, K. O., and Cheng, R. K., 2005, "A Comparison of the Flowfields and Emissions of High-Swirl Injectors and Low-Swirl Injectors for Lean Premixed Gas Turbines," Proc. Combust. Inst., 30, pp. 2867-2874.

(3) Littlejohn, D., and Cheng, R. K., 2007, "Fuel Effects on a Low-Swirl Injector for Lean Premixed Gas Turbines," Proc. Combust. Inst., **31**(2), pp. 3155-3162.

(4) Cheng, R. K., Littlejohn, D., Nazeer, W. A., and Smith, K. O., 2008, "Laboratory Studies of the Flow Field Characteristics of Low-Swirl Injectors for Application to Fuel-Flexible Turbines," ASME J. Eng. Gas Turbines Power, 130, 021501.
(5) Littlejohn, D., Cheng, R. K., Noble, D. R., and Lieuwen, T., 2010, "Laboratory Investigations of Low-Swirl Injectors Operating with Syngases," Journal of Eng. for Gas Turbines and Power, **132**, 011502-1
(6) Glarborg, P., Miller, J.A., and Kee, R.J., 1986, "Kinetic Modeling and Sensitivity Analysis of Nitrogen Oxide Formation in Well-Stirred Reactors," Combustion and Flame, **65**, pp. 177-202.
(7) Smith, G. P., Golden, D. M., Frenklach, M., Moriarty, N. W., Eiteneer, B., Goldenberg, M., Bowman, C. T., Hanson, R. K., Song, S., Gardiner, W. C. Jr., Lissianski, V. V., and Qin, Z., http://www.me.berkeley.edu/gri_mech/
(8) Dooley, S., Burke, M.P., Chaos, M., Stein, Y., Dryer, F.L., Zhukov, V. P., Finch, O., Simmie, J.M., and Curran, H.J., 2010, "Methyl Formate Oxidation: Speciation Data, Laminar Burning Velocities, Ignition Delay Times, and a Validated Chemical Kinetic Model," Int. J. Chem Kin., **42**, pp 527-549.
(9) Healy, D., Kalitan, D. M., Aul, C. J., Petersen, E.L., Bourque, G., and Curran, H. J., 2010, "Oxidation of C1-C5 Alkane Quinternary Natural Gas Mixtures at High Pressures Energy and Fuels," Energy and Fuels, **24**, pp. 1521-1528.
(10) Umanskii, S., Bryukov, M., Strelkova, M., and I Chernysheva, 2009, ''Kintech Mechanism,'' Private Communication.
(11) Ranzi, E., Dente, M., Goldaniga, A., Bozzano, G., Faravelli, T., 2001, "Lumping Procedures in Detailed Kinetic Modelling of Gasification, Pyrolysis, Partial Oxidation and Combustion of Hydrocarbon Mixtures," Prog. Energy Combust. Sci., **27**, pp. 99-139.
(12) Wang, H., You., X., Joshi, A. V., Davis, S. G., Laskin, A., Egolfopoulos, F., and Law, C. K., 2007, "USC Mech Version II. High-Temperature Combustion Reaction Model of H2/CO/C1-C4 Compounds," http://ignis.usc.edu/USC_Mech_II.htm
(13) Lefebvre, A. H., "Gas Turbine Combustion," pp. 328-330, Taylor & Francis Group, New York, 1999.